

Critical Particle Sizes for the Engulfment of Nanoparticles by Membranes and Vesicles with Bilayer Asymmetry – Supporting Information

Jaime Agudo-Canalejo and Reinhard Lipowsky*

*Theory & Biosystems, Max Planck Institute of Colloids and Interfaces,
14424 Potsdam, Germany*

E-mail: lipowsky@mpikg.mpg.de

This Supporting Information contains technical details about

- A. Free energy landscapes for engulfment process, with Figures S1 and S2;
- B. Exocytic engulfment of nanoparticles, with Figure S3; and
- C. Spreading dynamics and engulfment rate.

Figure S1 depicts the basic geometry of the vesicle-particle system for endocytic engulfment. Figure S2 illustrates the different free energy landscapes for the engulfment process, emphasizing the landscapes for the bistable regime \mathcal{B}_{st} . Figure S3 shows the four engulfment regimes for exocytic engulfment by weakly curved membranes as a function of particle size and spontaneous curvature.

A. Free Energy Landscapes for Engulfment Process

Geometry of bound and unbound membrane segments. In order to minimize the free energy of the vesicle-particle system, we decomposed the membrane into a bound seg-

*To whom correspondence should be addressed

ment and an unbound segment as shown in Figure S1 for endocytic engulfment. The bound membrane segment (red in Figure S1) is in contact with the nanoparticle of radius R_{pa} and extends up to the contact line which defines the wrapping angle ϕ . This angle varies from $\phi = 0$ for the free particle state to $\phi = \pi$ for the completely engulfed state and can be regarded as the reaction coordinate for the engulfment process. The total membrane area $A = 4\pi R_{\text{ve}}^2$ is equal to the sum of the area A_{bo} of the bound membrane segment and the area A_{un} of the unbound segment.

The bound segment of the vesicle membrane follows the contour of the particle, and thus assumes the shape of a spherical cap with mean curvature $M = \mp 1/R_{\text{pa}}$ where the minus and plus sign corresponds to the endocytic and exocytic process, respectively (main text, Figure 2). The area of the bound segment is given by

$$A_{\text{bo}} = 2\pi R_{\text{pa}}^2 (1 - \cos \phi). \quad (\text{S1})$$

If we cut the spherical particle along the contact line, we obtain two spherical caps. The spherical cap adjacent to the bound membrane segment has the volume

$$V_{\text{bo}} = \frac{4\pi}{3} R_{\text{pa}}^3 (2 + \cos \phi) [\sin(\phi/2)]^4. \quad (\text{S2})$$

The unbound membrane segment does not experience molecular interactions with the particle and its shape is determined (i) by the location of the contact line, which provides the circular boundary of the unbound membrane segment, (ii) by the area $A_{\text{un}} = A - A_{\text{bo}}$ of the unbound segment, (iii) by the effective volume $V \pm V_{\text{bo}}$, which is enclosed by the unbound membrane segment and the additional planar surface that spans the circular contact line, where the plus and minus sign applies to endo- and exocytosis, respectively; and (iv) by the spontaneous curvature m .

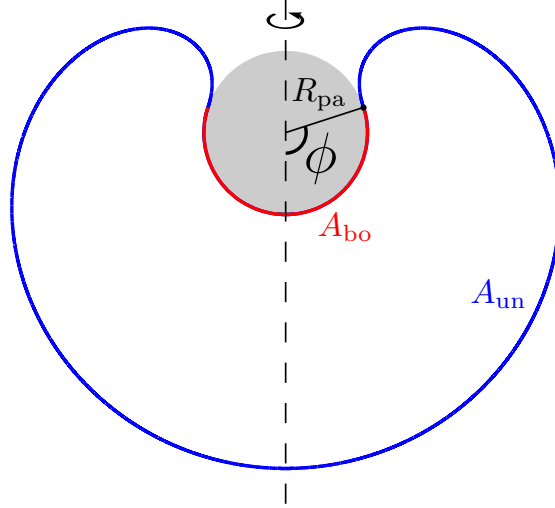


Figure S1: Vesicle membrane (red-blue) in contact with a spherical nanoparticle (gray) of radius R_{pa} . The vesicle shape is axially symmetric with respect to the vertical dashed line. The wrapping (or spreading) angle ϕ denotes the position of the contact line which partitions the membrane into a bound (red) and an unbound (blue) segment. The wrapping angle varies from $\phi = 0$ for the onset of adhesion up to $\phi = \pi$ for the completely engulfed state. The bound and unbound membrane segment have the areas A_{bo} and $A_{\text{un}} = A - A_{\text{bo}}$, respectively.

Decomposition of total free energy. As explained in the *Methods* section, the total free energy E is equal to the sum of the membrane's bending free energy E_{be} (main text, eq 21) and the adhesion free energy $E_{\text{ad}} = -|W| A_{\text{bo}}$. The total free energy can also be decomposed according to

$$E = E_{\text{bo}} + E_{\text{un}} \quad (\text{S3})$$

with the free energy

$$E_{\text{bo}} \equiv [-2\pi|W|R_{\text{pa}}^2 + 4\pi\kappa(1 \pm mR_{\text{pa}})^2] [1 - \cos(\phi)]. \quad (\text{S4})$$

of the bound membrane segment, where the plus and minus sign correspond to endocytic and exocytic engulfment, respectively, and the free energy

$$E_{\text{un}} = \int dA_{\text{un}} 2\kappa(M - m)^2 \quad (\text{S5})$$

of the unbound membrane segment where the integral extends over the area $A_{\text{un}} = A - A_{\text{bo}}$ of the latter segment.

In eq S4, we used the convention that the upper and lower sign of the \pm symbol corresponds to the endocytic and exocytic case, respectively. The same convention will be used below in all equations in which a \pm symbol appears.

Free energy minimization. In order to find the shape of the unbound segment that minimizes E_{un} for a given value of the wrapping angle ϕ and, thus, for a given location of the contact line, we minimize the shape functional

$$F_{\text{un}} \equiv E_{\text{un}} + \Sigma(A - A_{\text{bo}}) - \Delta P(V \pm V_{\text{bo}}) \quad (\text{S6})$$

where Σ and ΔP are Lagrange multipliers which ensure that the membrane area has the prescribed value A and that the unbound and bound membrane together enclose the vesicle volume V . The auxiliary volume $V \pm V_{\text{bo}}$ is enclosed by the unbound membrane segment and the additional planar surface that spans the circular contact line. When we calculate the free energy $E_{\text{un}}(\phi)$ of the unbound membrane segment by minimizing the shape functional F_{un} in eq S6 for many different values of ϕ within the interval $0 < \phi < \pi$, keeping both the area A and the volume V fixed, we obtain the corresponding free energy landscape

$$E(\phi) = [-2\pi|W|R_{\text{pa}}^2 + 4\pi\kappa(1 \pm mR_{\text{pa}})^2] [1 - \cos(\phi)] + E_{\text{un}}(\phi) \quad (\text{S7})$$

where the first term on the right hand side follows from eq S4. Typical free energy landscapes $E(\phi)$ obtained in this way are displayed in Figure S2 corresponding to the parameter values marked with green diamonds in Figure 3c. In general, the free energy landscapes may contain additional minima corresponding to additional intermediate states. For the uniform membranes considered in the main text, these additional states can always be ignored because they represent satellite minima very close to the free or completely engulfed states, from

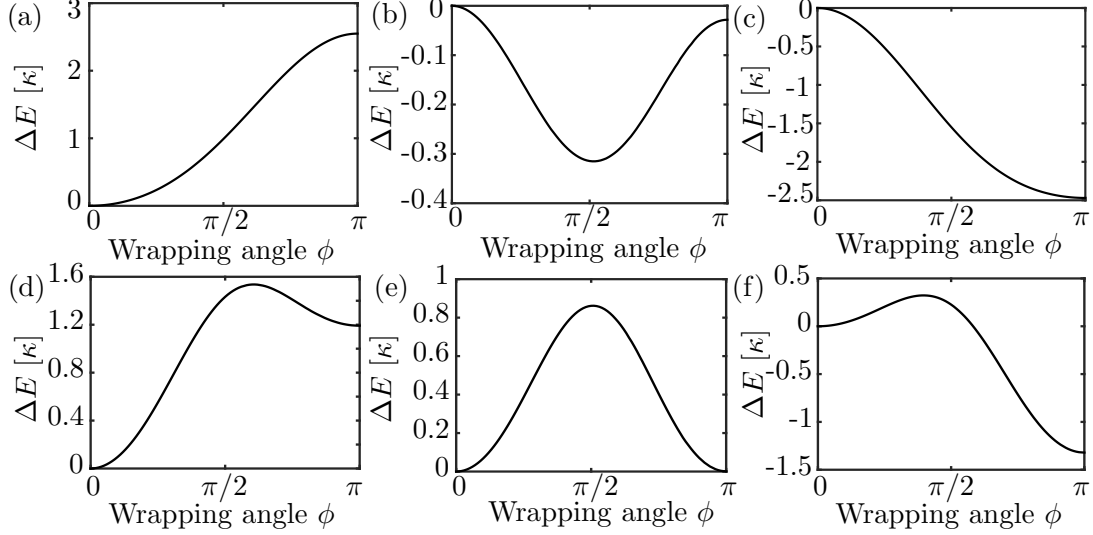


Figure S2: Free energy landscapes $\Delta E(\phi) \equiv E(\phi) - E(0)$ corresponding to the six parameter values marked by green diamonds in Figure 3c: (a) For the free (or non-engulfment) regime \mathcal{F}_{st} , the landscape has a minimum at $\phi = 0$, which corresponds to the free state \mathcal{F} , and a maximum at $\phi = \pi$, which defines the completely engulfed state \mathcal{C} ; (b) For the partial engulfment regime \mathcal{P}_{st} , the landscape has maxima both at $\phi = 0$ and at $\phi = \pi$ and a minimum at an intermediate ϕ -value corresponding to a partially engulfed state; (c) For the complete engulfment regime \mathcal{C}_{st} , the landscape exhibits a minimum at $\phi = \pi$ and a maximum at $\phi = 0$; (d, e, f) Three landscapes within the bistable regime \mathcal{B}_{st} with two local minima at $\phi = 0$ and $\phi = \pi$ separated by a free energy barrier. In panels (d) and (f), the global minima are provided by the states \mathcal{F} and \mathcal{C} , respectively. Panel (e) corresponds to the transition line L_* at which both states \mathcal{F} and \mathcal{C} have the same free energy.

which they are separated by tiny energy barriers that can be easily overcome by thermal fluctuations.

Free energy landscape close to free particle state \mathcal{F} . Close to the free particle state \mathcal{F} with $\phi = 0$, the free energy landscape behaves as

$$E(\phi) \approx E(0) + \frac{1}{2} E'' \phi^2 \quad \text{with} \quad E'' \equiv \left. \frac{d^2 E(\phi)}{d\phi^2} \right|_{\phi=0}. \quad (\text{S8})$$

The free particle state is (meta)stable as long as $E'' > 0$ and unstable for $E'' < 0$, which implies that $E'' = 0$ determines the instability line L_{fr} . Using the decomposition $E = E_{\text{bo}} + E_{\text{un}}$ of the free energy into the contributions from the bound and unbound membrane

segments, as in eqs S3 - S5, we obtain $E'' = E''_{\text{bo}} + E''_{\text{un}}$ with

$$E''_{\text{bo}} = -2\pi R_{\text{pa}}^2 |W| + 4\pi\kappa(1 \pm R_{\text{pa}} m)^2 \quad (\text{S9})$$

with the plus (minus) sign corresponding to endocytosis (exocytosis).

The instability line L_{fr} is now determined by

$$E'' = -2\pi R_{\text{pa}}^2 |W| + 4\pi\kappa(1 \pm R_{\text{pa}} m)^2 + E''_{\text{un}} = 0. \quad (\text{S10})$$

Alternatively, we may also determine L_{fr} from the instability relation

$$M_{\text{co}} = M_{\text{ms}} \quad \text{or} \quad \sqrt{R_{\text{pa}}^2 |W| / (2\kappa)} = 1 \pm R_{\text{pa}} M_{\text{ms}} \quad (\text{S11})$$

where the expression for the contact mean curvature M_{co} in eq 23 of the main text has been used. The two relationships as given by eqs S10 and S11 are only equivalent if the unbound membrane segment makes the contribution

$$E''_{\text{un}} = 4\pi\kappa R_{\text{pa}} [M_{\text{ms}} - m] [\pm 2 + R_{\text{pa}} (M_{\text{ms}} + m)] \quad (\text{S12})$$

to the second derivative E'' . A combination of E''_{bo} in eq S9 and E''_{un} in eq S12 then leads to

$$E'' = E''_{\text{bo}} + E''_{\text{un}} = -2\pi R_{\text{pa}}^2 |W| + 4\pi\kappa(1 \pm R_{\text{pa}} M_{\text{ms}})^2. \quad (\text{S13})$$

For endocytosis (+ sign), this relationship is identical to eq 6 in the main text.

Relation between membrane area and mechanical membrane tension. In the theoretical approach used here, the mechanical tension Σ does not represent an independent parameter but plays the role of a Lagrange multiplier Σ , see eq S6, which is determined in terms of the other parameters in order to ensure that the membrane area has the prescribed

value A .¹⁻³ The minimization procedure typically leads to Lagrange multipliers Σ that correspond to relatively small tensions of the order of κ/R_{ve}^2 , $\kappa m/R_{ve}$, or κm^2 . If we stretched the membrane with such a tension, the change in membrane area arising from the membrane's area compressibility would be rather small which provides a consistency check on the theory. In fact, even in the presence of relatively large tensions of the order of 1 mN/m, the membrane area can only change by a few percent without rupturing. Thus, as long as the membrane does not rupture, its area remains constant to a very good approximation. For giant unilamellar vesicles (GUVs), the membrane area A can be directly measured and it is then possible to corroborate the theory by a systematic comparison of calculated and experimentally observed membrane shapes as has been successfully done for lipid vesicles in the absence of nanoparticles.⁴⁻⁶

An alternative theoretical approach has been used in refs 7 and 8 where the engulfment of nanoparticles was theoretically studied in the presence of a certain prescribed membrane tension Σ' . This tension was treated as an independent control parameter and then represents a 'chemical potential' for membrane area which would govern the exchange of area with a putative area reservoir, in analogy to a grand-canonical ensemble. This approach is motivated by the view that eukaryotic cells control the tension of their plasma membranes, presumably by regulating the osmotic conditions and by remodelling the cytoskeletal forces acting on the cell membrane, which leads to the so-called cortical tension. Because the mechanisms underlying this tension are complex and poorly understood, it is appealing to reduce this complexity to a single tension parameter. One difficulty with this approach is that the measured tension values are quite variable and change during the cell cycle. Indeed, recent experiments provide Σ' -values in the range between 0.05 and 2 mN/m.^{9,10} Another difficulty is that the actin-myosin cortex exerts complex patterns of forces onto the cell membrane which contribute to the membrane tension but, at the same time, directly affect the membrane shape, and it is not obvious that these two effects of the cortical forces may be decomposed and considered separately.

The lipid membranes and vesicles addressed in our study do not involve an area (or lipid) reservoir which implies that the membrane area A rather than the membrane tension should be regarded as the basic control parameter. Furthermore, the instability relations for the free and completely engulfed particle states as derived here depend only on *local* properties of the membrane close to the nanoparticle and can, thus, also be applied to cell membranes. In fact, one can show that the free energy landscapes for particle engulfment remain unaffected by small tensions $\Sigma' \ll \Sigma_o \equiv \kappa/R_{\text{pa}}^2$. For a membrane with a clathrin coat, the bending rigidity is $\kappa = 10^{-18}$ J as measured in ref 11 which leads to crossover tensions $\Sigma_o \geq 0.4$ mN/m for particle sizes $R_{\text{pa}} \leq 50$ nm as studied experimentally in refs 12 and 13.

B. Exocytic Engulfment of Nanoparticles

Instability relations for exocytic engulfment. For exocytic engulfment, the curvature M_{ms} of the membrane segment adjacent to the free particle state \mathcal{F} (main text, Figure 5) must be smaller than $1/R_{\text{pa}}$ in order to ensure that the membrane and the particle do not intersect each other. Furthermore, the contact mean curvature is given by $M_{\text{co}} = -\frac{1}{R_W} + \frac{1}{R_{\text{pa}}}$ as explained in the *Methods* section. As a consequence, the relation $M_{\text{co}} = M_{\text{ms}}$ for the instability line L_{fr} of the free state \mathcal{F} leads to

$$R_{\text{pa}} = R_{\text{fr}} \equiv \frac{1}{M_{\text{ms}} + R_W^{-1}} \quad \text{and} \quad M_{\text{ms}} > -1/R_W \quad (L_{\text{fr}}, \text{exocytosis}). \quad (\text{S14})$$

and the membrane segment starts to spread over the particle if

$$R_{\text{pa}} > R_{\text{fr}} \quad \text{and} \quad M_{\text{ms}} > -1/R_W \quad (\text{unstable } \mathcal{F}, \text{exocytosis}). \quad (\text{S15})$$

For strongly curved membrane segments with a negative mean curvature M_{ms} smaller than $-1/R_W$, the free state \mathcal{F} is stable for all particle sizes, *i.e.*, the critical particle size $R_{\text{fr}} = \infty$.

For exocytic engulfment, the curvature M'_{ms} of the mother membrane adjacent to the

membrane neck of the completely engulfed state \mathcal{C} (main text, Figure 6) must be larger than $-1/R_{\text{pa}}$ in order to ensure that the mother membrane does not intersect the membrane segment bound to the particle. The instability line L_{ce} for the state \mathcal{C} as determined by $M_{\text{co}} + M'_{\text{ms}} = 2m$ now has the form

$$R_{\text{pa}} = R_{\text{ce}} \equiv \frac{1}{2m + R_W^{-1} - M'_{\text{ms}}} \quad \text{for} \quad M'_{\text{ms}} < 2m + 1/R_W \quad (L_{\text{ce}}, \text{exocytosis}), \quad (\text{S16})$$

and the membrane neck starts to open if

$$R_{\text{pa}} < R_{\text{ce}} \quad \text{and} \quad M'_{\text{ms}} < 2m + 1/R_W \quad (\text{unstable } \mathcal{C}, \text{exocytosis}). \quad (\text{S17})$$

If the unbound membrane segment has a mean curvature M'_{ms} larger than $2m + \frac{1}{R_W}$, the completely engulfed state \mathcal{C} is unstable for all particle sizes, *i.e.*, $R_{\text{ce}} = \infty$. The physical requirement that the membrane has no self-intersections in state \mathcal{C} leads to the additional condition that M'_{ms} is larger than $-1/R_{\text{pa}}$. Therefore, stable states \mathcal{C} without self-intersections are only possible for $-\frac{1}{R_{\text{pa}}} < M'_{\text{ms}} < 2m + \frac{1}{R_W}$.

These instability lines and instability criteria for exocytic engulfment can be transformed into those for endocytic engulfment, if we change (i) the sign of the spontaneous curvature m as well as (ii) the signs of the curvatures M_{ms} and M'_{ms} of the two membrane segments. This ‘mirror symmetry’ implies that we have a one-to-one correspondence between the engulfment diagrams for exocytic and endocytic engulfment as illustrated further below for the case of weakly curved membranes.

For notational simplicity, we have used the same notation R_W for the adhesion length of both the endocytic and the exocytic process. Note, however, that the two adhesion lengths may have different numerical values because the molecular interactions described by the adhesive strength W may be different on the two sides of the asymmetric bilayer.

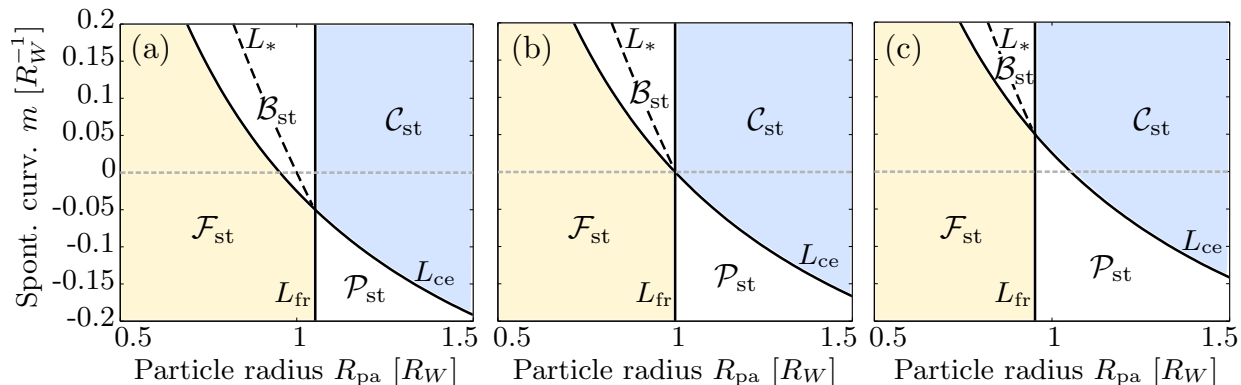


Figure S3: Exocytic engulfment of nanoparticles by weakly curved membranes: Different engulfment regimes \mathcal{F}_{st} , \mathcal{B}_{st} , \mathcal{C}_{st} and \mathcal{P}_{st} as a function of particle size R_{pa} and spontaneous curvature m , both measured in units of the adhesion length R_W . (a) Concave membrane segments with small negative curvatures $M_{\text{ms}} = M'_{\text{ms}} = -0.05/R_W$; (b) Flat membrane segments with vanishing curvatures $M_{\text{ms}} = M'_{\text{ms}} = 0$; and (c) Convex membrane segments with small positive curvatures $M_{\text{ms}} = M'_{\text{ms}} = +0.05/R_W$. The two instability lines L_{fr} and L_{ce} for the free and completely engulfed states are given by eq S14 and eq S16 and define the critical particle sizes R_{fr} and R_{ce} . The bistable regimes \mathcal{B}_{st} contain the transition lines L_* (dashed) at which the free and completely engulfed states coexist. All four engulfment regimes meet at the ‘multicritical’ intersection points of the two instability lines. Compared to endocytic engulfment (main text, Figure 7), the relative locations of the regimes \mathcal{B}_{st} and \mathcal{P}_{st} have been swapped.

Critical particle sizes for exocytic engulfment. The equations of the previous subsection imply that the intersection point of the two instability lines is again located at $m = \frac{1}{2}(M_{\text{ms}} + M'_{\text{ms}})$ but that the relative positions of the intermediate size regimes \mathcal{B}_{st} and \mathcal{P}_{st} are now swapped compared to the endocytic case. Therefore, the engulfment process is continuous for $m < \frac{1}{2}(M_{\text{ms}} + M'_{\text{ms}})$ and discontinuous for $m > \frac{1}{2}(M_{\text{ms}} + M'_{\text{ms}})$, see Table S1. The latter table also contains the two critical particle radii for exocytic engulfment as obtained from the corresponding instability criteria in eqs S15 and S17.

Exocytic engulfment by weakly curved mother membranes. For sufficiently large values of the vesicle size R_{ve} , the two membrane curvatures M_{ms} and M'_{ms} can again be neglected. The corresponding engulfment diagram is depicted in Figure S3b as a function of particle size R_{pa} and spontaneous curvature m , both measured in units of the adhesion length

Table S1: Critical particle sizes for *exocytic* engulfment as derived from eqs S15 and S17.

Range of spontaneous curvature m	Intermediate size regime	Engulfment process	Lower critical size	Upper critical size
$m > \frac{1}{2} (M_{\text{ms}} + M'_{\text{ms}})$	bistable \mathcal{B}_{st}	discontinuous	R_{ce}	R_{fr}
$m < \frac{1}{2} (M_{\text{ms}} + M'_{\text{ms}})$	partial \mathcal{P}_{st}	continuous	R_{fr}	R_{ce}

R_W . Inspection of Figure S3b shows that exocytic engulfment by flat membranes leads to partially engulfed states for negative spontaneous curvature and to bistability for positive spontaneous curvature. This behavior for the exocytic process is exactly the opposite of the behavior for the endocytic process for which partially engulfed states occur for positive spontaneous curvature and bistability is found for negative spontaneous curvatures (main text, Figure 7b). For small but finite values of the segment curvatures M_{ms} and M'_{ms} , the regimes for exocytic engulfment again undergo small changes, primarily determined by the sign of $M_{\text{ms}} + M'_{\text{ms}}$, as illustrated in Figure S3a and Figure S3c.

A detailed comparison of the different regimes for exocytic and endocytic engulfment as displayed in Figure S3 and Figure 7 shows that the exocytic diagrams can be obtained from the endocytic ones if we simultaneously change the sign of the spontaneous curvature m as well as the signs of the segment curvatures M_{ms} and M'_{ms} . In this way, we obtain Figure S3c from Figure 7a and Figure S3a from Figure 7c. This ‘mirror symmetry’ of the engulfment diagrams is a direct consequence of the corresponding ‘mirror symmetry’ of the instability criteria as pointed out after eq S17.

Adhesion length and spontaneous curvature from critical particle sizes. If the exocytic engulfment process is continuous and proceeds *via* partially engulfed states, the two critical particle sizes R_{fr} and $R_{\text{ce}} > R_{\text{fr}}$ are accessible to direct observation, either in experimental or in simulations studies. From the observed critical sizes, we can then

determine the adhesion length *via*

$$R_W = \frac{R_{\text{fr}}}{1 - R_{\text{fr}} M_{\text{ms}}} \quad (\text{cont exocytosis}) \quad (\text{S18})$$

and the spontaneous curvature *via*

$$m = \frac{1}{2} \left[\frac{1}{R_{\text{ce}}} - \frac{1}{R_{\text{fr}}} + M_{\text{ms}} + M'_{\text{ms}} \right] \quad (\text{cont exocytosis}) \quad (\text{S19})$$

as follows from eqs S14 and S16.

C. Kinetics of Membrane Spreading and Engulfment Rate

Force balance at the contact line. The spreading of the membrane over the particle surface is induced by the attractive membrane-particle forces and proceeds *via* the displacement of the contact line. For the engulfment of a spherical particle, the membrane geometry is axially symmetric and the contact line has the total length

$$L_{\text{co}} = 2\pi R_{\text{pa}} \sin(\phi). \quad (\text{S20})$$

The position of the contact line is determined by the contact point of the membrane contour.

The coordinate of this point is taken to be the arc length

$$s \equiv R_{\text{pa}} \phi \quad (\text{S21})$$

of the bound membrane contour measured from the south pole of the particle with $\phi = 0$ as in Figure S1. The displacement of the contact line now corresponds to changes in s .

The contact line at position s experiences two forces: a thermodynamic driving force and a friction force. The thermodynamic driving force F_1 reflects the change in the system's

energy as we displace the contact line. This force has the form

$$F_1 = -\frac{dE_s(s)}{ds} = -\frac{1}{R_{\text{pa}}}\frac{dE(\phi)}{d\phi} \quad (\text{S22})$$

where $E_s(s)$ is the free energy landscape of the system as a function of s , *i.e.*, $E_s(s) = E(\phi(s)) = E(s/R_{\text{pa}})$ with the free energy landscape $E(\phi)$ as discussed before, see Figure S2. The force F_2 , on the other hand, depends on the dissipation mechanism. If the contact line does not move, there will be no friction. Therefore, the friction force F_2 is taken to be proportional to the velocity $v = ds/dt$ of the contact line which is equal to the derivative of arc length s with respect to time t . The friction coefficient for the displacement of the whole contact line should be proportional to the length L_{co} of the contact line which implies $F_2 = \eta_{\text{eff}}L_{\text{co}}ds/dt$ which defines the effective dynamic viscosity η_{eff} . Using eq S20 for the contact length L_{co} and changing variables from arc length s to wrapping angle ϕ *via* $s = R_{\text{pa}}\phi$, we obtain the ϕ -dependent friction force

$$F_2 = 2\pi\eta_{\text{eff}}R_{\text{pa}}^2\sin(\phi)\frac{d\phi}{dt}. \quad (\text{S23})$$

We now balance the thermodynamic driving force F_1 in eq S22 with the friction force F_2 in eq S23, *i.e.*, we set $F_1 = F_2$ which leads to the equation of motion for the contact line as given by

$$\sin(\phi)\frac{d\phi}{dt} = -\frac{1}{2\pi\eta_{\text{eff}}R_{\text{pa}}^3}\frac{dE(\phi)}{d\phi} \quad (\text{S24})$$

which is identical with eq 17 in the main text.

Size-dependent engulfment rate. The equation of motion for the contact line (eq S24) involves the gradient $dE/d\phi$ of the free energy landscape which can again be decomposed into two contributions from the bound and unbound membrane segment, *i.e.*,

$$\frac{dE(\phi)}{d\phi} = \frac{dE_{\text{bo}}(\phi)}{d\phi} + \frac{dE_{\text{un}}(\phi)}{d\phi} \quad (\text{S25})$$

with

$$\frac{d E_{\text{bo}}(\phi)}{d \phi} = [-2\pi|W|R_{\text{pa}}^2 + 4\pi\kappa_{\text{bo}}(1 \pm m_{\text{bo}} R_{\text{pa}})^2] \sin(\phi) \quad (\text{S26})$$

with the plus sign corresponding to endocytosis.

As far as the gradient $d E_{\text{un}}(\phi)/d \phi$ of the unbound membrane (or mother membrane) is concerned, it is intuitively plausible that $E_{\text{un}}(\phi)$ changes primarily by shape changes of the unbound membrane segment close to the contact line and that these changes are small if this segment can adapt its mean curvature to the spontaneous curvature m . For $m = 0$, for example, this segment can attain a shape close to a catenoid which has vanishing bending energy and, thus, makes no contribution to E_{un} . This expectation can be directly confirmed for the initial spreading close to the free state \mathcal{F} , *i.e.*, for small values of the wrapping angle ϕ because

$$\frac{d E_{\text{un}}(\phi)}{d \phi} \approx E''_{\text{un,fr}} \phi = 4\pi\kappa R_{\text{pa}}[M_{\text{ms}} - m] [\pm 2 + R_{\text{pa}}(M_{\text{ms}} + m)] \phi \quad \text{for small } \phi \quad (\text{S27})$$

as follows from $E_{\text{un}}(\phi) \approx E_{\text{un}}(0) + \frac{1}{2} E''_{\text{un,fr}} \phi^2$ and eq S12 with $E''_{\text{un}} = E''_{\text{un,fr}}$. The latter equation also applies to the present case because the unbound membrane segment (or mother membrane) is characterized by the same fluid-elastic parameters m and κ as in the case of the uniform membrane.

Likewise, for the final spreading process close to the completely engulfed state \mathcal{C} , *i.e.*, for small deviations $\delta\phi \equiv \phi - \pi$, the free energy landscape for the unbound membrane segment behaves as $E_{\text{un}}(\phi) \approx E_{\text{un}}(\pi) + \frac{1}{2} E''_{\text{un,ce}} \delta\phi^2$ with

$$E''_{\text{un,ce}} \equiv \left. \frac{d^2 E_{\text{un}}(\phi)}{d \phi^2} \right|_{\phi=\pi} = 4\pi\kappa R_{\text{pa}}[M'_{\text{ms}} - m] [\pm 2 + R_{\text{pa}}(3m - M'_{\text{ms}})]. \quad (\text{S28})$$

which implies the gradient

$$\frac{d E_{\text{un}}(\phi)}{d \phi} \approx 4\pi\kappa R_{\text{pa}}(M'_{\text{ms}} - m) [\pm 2 + R_{\text{pa}}(3m - M'_{\text{ms}})] \delta\phi \quad \text{for small } \delta\phi. \quad (\text{S29})$$

Inspection of eqs S27 and S29 shows that the gradient $dE_{\text{un}}(\phi)/d\phi$ is proportional to $R_{\text{pa}}(M_{\text{ms}} - m)$ for small ϕ and to $R_{\text{pa}}(M'_{\text{ms}} - m)$ for small $\delta\phi = \phi - \pi$. These dependencies have two implications. First, the gradient $dE_{\text{un}}(\phi)/d\phi$ vanishes for small ϕ and $M_{\text{ms}} = m$ as well as for small $\delta\phi$ and $M'_{\text{ms}} = m$ as expected. Second, this gradient becomes small if both the segment curvatures M_{ms} and M'_{ms} as well as the spontaneous curvature m are small compared to the inverse particle radius $1/R_{\text{pa}}$. The latter property motivates a systematic expansion of the free energy E_{un} in powers of the size ratio $\epsilon \equiv R_{\text{pa}}/R_{\text{ve}}$ with $R_{\text{ve}} = \sqrt{A/4\pi}$ as before. Such an expansion shows (i) that $M'_{\text{ms}} \approx M_{\text{ms}}$ to leading order in ϵ and (ii) that the free energy gradient $dE_{\text{un}}/d\phi$ of the unbound membrane segment behaves as

$$\frac{dE_{\text{un}}(\phi)}{d\phi} = \pm 8\pi\kappa R_{\text{pa}}(M_{\text{ms}} - m) \sin(\phi) \cos(\phi) + \mathcal{O}(\epsilon^2). \quad (\text{S30})$$

For small values of ϕ and $\delta\phi = \phi - \pi$, this expression becomes identical, to first order in $\epsilon = R_{\text{pa}}/R_{\text{ve}}$, with eq S27 and eq S29, respectively. This asymptotic behavior has been confirmed by numerical minimization of the total free energy. Therefore, in the limit of small size ratios $R_{\text{pa}}/R_{\text{ve}}$, the gradient $dE_{\text{un}}(\phi)/d\phi$ is proportional to $R_{\text{pa}}(M_{\text{ms}} - m) \approx R_{\text{pa}}(M'_{\text{ms}} - m)$ for all values of ϕ . As a consequence, this gradient can be neglected if both the segment curvatures M_{ms} and M'_{ms} as well as the spontaneous curvature m are much smaller than the inverse particle radius $1/R_{\text{pa}}$. In the latter case, the gradient of the free energy landscape is determined by the bound membrane segment alone and behaves as

$$\frac{dE(\phi)}{d\phi} \approx \frac{dE_{\text{bo}}(\phi)}{d\phi} = [-2\pi|W|R_{\text{pa}}^2 + 4\pi\kappa_{\text{bo}}(1 \pm m_{\text{bo}}R_{\text{pa}})^2] \sin(\phi) \quad (\text{S31})$$

as follows from eq S26. When we insert this expression for $dE(\phi)/d\phi$ into the equation of motion as given by eq S24 (or eq 17 in the main text), the factors proportional to $\sin(\phi)$ cancel and we obtain the simplified equation of motion

$$\frac{d\phi}{dt} = \frac{|W|R_{\text{pa}}^2 - 2\kappa(1 \pm mR_{\text{pa}})^2}{\eta_{\text{eff}} R_{\text{pa}}^3} \quad (\text{S32})$$

which implies that the wrapping velocity $d\phi/dt$ is constant and that the engulfment time $t_{\mathcal{FC}}$ follows from

$$\pi = \frac{|W|R_{\text{pa}}^2 - 2\kappa(1 \pm mR_{\text{pa}})^2}{\eta_{\text{eff}} R_{\text{pa}}^3} t_{\mathcal{FC}}. \quad (\text{S33})$$

For the plus sign corresponding to endocytosis, eq S33 is equivalent to eq 18 in the main text.

References

- (1) Deuling, H.; Helfrich, W. The Curvature Elasticity of Fluid Membranes: A Catalogue of Vesicle Shapes. *J. Physique* **1976**, *37*, 1335–1345.
- (2) Seifert, U.; Berndl, K.; Lipowsky, R. Shape Transformations of Vesicles: Phase Diagram for Spontaneous Curvature and Bilayer Coupling Model. *Phys. Rev. A* **1991**, *44*, 1182–1202.
- (3) Lipowsky, R. Coupling of Bending and Stretching Deformations in Vesicle Membranes. *Adv. Colloid Interface Sci.* **2014**, *208*, 14–24.
- (4) Berndl, K.; Käs, J.; Lipowsky, R.; Sackmann, E.; Seifert, U. Shape Transformations of Giant Vesicles: Extreme Sensitivity to Bilayer Asymmetry. *Europhys. Lett.* **1990**, *13*, 659–664.
- (5) Lipowsky, R. The Conformation of Membranes. *Nature* **1991**, *349*, 475–481.
- (6) Döbereiner, H.-G.; Evans, E.; Kraus, M.; Seifert, U.; Wortis, M. Mapping Vesicle Shapes into the Phase Diagram: A Comparison of Experiment and Theory. *Phys. Rev. E* **1997**, *55*, 4458 – 4474.
- (7) Deserno, M. Elastic Deformation of a Fluid Membrane upon Colloid Binding. *Phys. Rev. E* **2004**, *69*, 031903.

- (8) Zhang, S.; Li, J.; Lykotrafitis, G.; Bao, G.; Suresh, S. Size-Dependent Endocytosis of Nanoparticles. *Adv. Mater.* **2009**, *21*, 419 – 424.
- (9) Tinevez, J.-Y.; Schulze, U.; Salbreux, G.; Roensch, J.; Joanny, J.-F.; Paluch, E. Role of Cortical Tension in Bleb Growth. *Proc. Nat. Acad. Sci. USA* **2009**, *106*, 18581–18586.
- (10) Fischer-Friedrich, E.; Hyman, A. A.; Jülicher, F.; Müller, D. J.; Helenius, J. Quantification of Surface Tension and Internal Pressure Generated by Single Mitotic Cells. *Scientific Rep.* **2014**, *4*, 6213.
- (11) Jin, A. J.; Prasad, K.; Smith, P. D.; Lafer, E. M.; Nossal, R. Measuring the Elasticity of Clathrin-Coated Vesicles *via* Atomic Force Microscopy. *Biophys. J.* **2006**, *90*, 3333 – 3344.
- (12) Chithrani, B. D.; Ghazani, A. A.; Chan, W. C. W. Determining the Size and Shape Dependence of Gold Nanoparticle Uptake into Mammalian Cells. *Nano Lett.* **2006**, *6*, 662 – 668.
- (13) Chithrani, B. D.; Chan, W. C. W. Elucidating the Mechanism of Cellular Uptake and Removal of Protein-Coated Gold Nanoparticles of Different Sizes and Shapes. *Nano Lett.* **2007**, *7*, 1542 – 1550.